A Novel Low-Cost H-Plane Decoupling Technique for Two Closely Placed Patch Antennas Using Electric and Magnetic Coupling Cancellation

Jianfeng Qian, *Graduate Student Member, IEEE*, Benito Sanz Izquierdo, *Member, IEEE*, Steven Gao, *Fellow, IEEE*, Hanyang Wang, *Fellow, IEEE*, Hai Zhou, and Huiliang Xu

***Abstract*— This article presents a novel low-cost method for decoupling two closely placed H-plane arranged patch antennas. This new electric and magnetic coupling cancellation (EMCC) decoupling concept is simple yet highly effective, requiring no additional decoupling structures or complicated manufacturing processes. According to the proposed concept, the mutual coupling between two patches can be suppressed by controlling the weight of the electric (E) and magnetic (H) coupling between them. When the E-coupling and H-coupling are comparable, a deep null will arise on the mutual coupling curve, resulting in high isolation in the band of interest. To validate the approach, two prototypes for both two-element and four-element multi-input multi-output (MIMO) arrays are designed, fabricated, and measured. The experimental results agree well with the simulations, highlighting the advantages of this method, including low cost, high isolation, and simple antenna structures.**

***Index Terms*— Cancellation, closely placed, decoupling, multi-input multi-output (MIMO), patch antenna.**

I. Introduction

As ONE of the most popular antenna types, patch antennas are widely used in many applications for their low cost, planar structure, low profile, and ease of fabrication. In a modern communication system, multiple antennas are integrated on the same printed circuit board for higher capacity or diversity purposes. However, the mutual coupling problem is always a bottleneck that limits the final achievable system performance. High mutual coupling can not only deteriorate the total efficiency of the system but also reduce the overall capacity. In extreme cases, the energy transmitted from one antenna to another can even damage the receiving transceiver.

To mitigate the mutual coupling between two patch antennas, extensive research has been conducted over the years. One common approach to improve the isolation is by reducing the surface wave coupling [1], [2], [3], [4], [5]. This concept is widely used when the patches are placed within a relatively large distance, where the surface wave dominates the mutual coupling. Alternatively, the mutual coupling can also be reduced by introducing a band-reject response in the band of interest by using interpatch loading elements, such as resonators [6], [7] and slot structures [8], [9], [10]. Additionally, the mutual coupling can be reduced by changing the coupling mode between the patches using structures, such as near-field resonators [11] and polarization conversion isolators [12]. Networks introducing another path to cancel the mutually coupled field are also a good option for mutual coupling reduction [13], [14], [15], [16], [17]. However, all these designs either need additional space for the implementation of decoupling structures or suffer from large antenna separations.

Some simple yet effective methods without using any additional decoupling structures are achieved by studying the natural field characteristics of patch antennas [18], [19], [20], [21], [22], [23], [24]. By intentionally designing antenna structures and arrangements in a specific manner, isolation between antenna ports can be achieved.

This article focuses on a special scenario, where two patch antennas are closely placed. It is well-known that as the distance between antenna elements decreases, the mutual coupling between them increases, particularly when they are in the same polarization. Additionally, the close proximity of the patches makes it challenging to implement complex decoupling structures between them.

In [9], two patch antennas are decoupled by cutting a resonating slot on the finite ground plane. This slot effectively traps the energy that would have coupled from one antenna to the other, resulting in improved isolation. However, this structure is sensitive to the ground plane size and may lead to high backside radiation [10]. Furthermore, cutting a slot on the ground is not ideal for many practical applications as it may interfere with devices mounted on the other side of the system board. In [11], closely packed patches are decoupled using an additional near-field resonating layer over the patches. With an edge-to-edge separation of 0.024 wavelength at the center frequency, 20-dB isolation is achieved. In [14], the mutual coupling between two closely placed patches is achieved by a simple metal strip coupled to both

Manuscript received 28 June 2023; revised 23 January 2024; accepted 15 February 2024. Date of publication 19 March 2024; date of current version 7 May 2024. This work was supported in part by Huawei Technology Ltd., and in part by the Royal Society-International Exchanges 2019 Cost Share (NSFC) under Grant IEC\NSFC\191780. *(Corresponding author: Jianfeng Qian.)*

Jianfeng Qian and Benito Sanz Izquierdo are with the School of Engineering and Digital Arts, University of Kent, CT2 7NT Canterbury, U.K. (e-mail: jq42@kent.ac.uk).

Steven Gao is with the Department of Engineering, The Chinese University of Hong Kong, Hong Kong.

Hanyang Wang, Hai Zhou, and Huiliang Xu are with Huawei Technology Ltd., RG2 6UF Reading, U.K.

Color versions of one or more figures in this article are available at https://doi.org/10.1109/TAP.2024.3376075.

Digital Object Identifier 10.1109/TAP.2024.3376075

patches. This coupled strip introduces an additional out-of-phase coupling path between the two antenna ports. With an edge-to-edge distance of $0.027\lambda_0$, the mutual coupling between the two ports is reduced to -18 dB. Unfortunately, the final achieved bandwidth is only 1.43%. In [20], two extremely closely placed patches are decoupled by making the patches operate over the higher order modes. At the cost of slightly reduced bandwidth and longer patches, a simple physical offset in the polarization direction can significantly improve the isolation up to 20 dB in the band of interest even when the antenna separation is only $0.007\lambda_0$ at its center frequency. A mode cancellation method is presented in [24] to reduce the mutual coupling between two closely packed patches. However, the presented examples only show isolations at the level of about 15 dB. In addition, for multielement multi-input multi-output (MIMO) scenarios, dummy patches are required to ensure a symmetric environment for the outer patches.

Up to now, most state-of-the-art decoupling techniques for closely packed antennas involve the use of additional decoupling structures [7], [8], [9], [10], [11], [14], [24], [25] or require extra space [20] for implementation. Some of them also suffer from small bandwidths, which are limited by the quality factors of resonant structures adopted in the decoupling process [9], [10], [11], [14]. To ensure a compact form factor, short design flow, and low cost, it is crucial to develop a simpler yet effective decoupling technique specifically for closely packed patch antennas.

In this article, a novel decoupling technique for two extremely closely placed patch antennas is presented. The proposed electric and magnetic coupling cancellation (EMCC) technique is based on the field analysis of the fundamental mode of a patch antenna. By cutting different regions at the nonradiating edges, the weight of electric and magnetic couplings between patches is adjusted. Then, it is found that the mutual coupling can be significantly reduced in the operating band by simply changing the dimensions of the cuts. Compared to other presented decoupling architectures, the proposed EMCC technique does not need any additional decoupling elements or complicated fabrication processes. To validate the effectiveness of our technique, we provide two example designs: a two-element MIMO array and a four-element MIMO array. Through our study, the proposed EMCC technique has the following advantages.

1) It can deal with extremely small antenna separation.

2) No additional decoupling element or complicated manufacturing process is needed, which means a simple structure, ease of fabrication, ease of design, and cost-efficient.

3) Small effect on the antennas' radiation performance, which means it is suitable for array applications too.

4) It can be applied to multielement MIMO arrays.

This article begins by introducing the design of a dual-antenna MIMO array. It focuses on analyzing the performance of a two-element MIMO system initially. Based on this structure, the mechanism of the proposed technique is studied in Section II-C. Then, according to the decoupling mechanism, the design philosophy of the technique is explained together with some parametric studies in Section II-D. In Section IV, this article discusses the application of the proposed decoupling technique to a larger antenna array. With all these results, the performance of the proposed technique is compared with other existing works in the field. Finally, Section IV concludes this article.

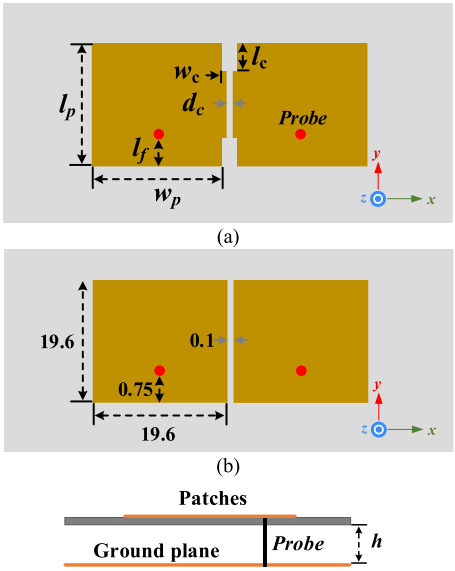

Fig. 1. Structure of the proposed decoupled patch antennas. (a) Decoupled patch antennas. (b) Reference design of coupled antennas with dimensions in mm. (c) Side view. Dimensions in mm: $l_f = 1.45$, $l_p = 21$, $l_c = 5$, $w_c = 0.2$, $w_p = 22$, $dc = 0.1$, and $h = 3$.

II. Two-Element MIMO Array

A. Antenna Structure

Fig. 1(a) depicts the physical structure of the proposed decoupled antennas, illustrating two patches placed in extremely close proximity. The distance between the two patches is set to 0.1 mm. The antennas are fed by a metal probe with a radius of 0.35 mm. The substrate employed in this design is Roger 4003, with a dielectric constant of 3.55, a loss tangent of 0.0027, and a thickness of 0.3 mm. Notably, Fig. 1(a) shows only two modified patch antennas without any additional decoupling elements. The only modification applied to the antennas involves cuts made at their corners. The specific design rules to decide the patch dimensions will be elaborated upon in Sections II-C-II-E.

B. Antenna Performance

According to classical antenna theory, the mutual coupling between patch antennas is closely associated with the separation distance between them [26], [27], [28], [29]. As the antennas are placed in closer proximity, the mutual coupling becomes stronger. In cases where the patches are positioned in an extremely small vicinity of each other, the mutual impedance has a significant impact on the impedance response of the coupled antennas.

First, a reference design without any decoupling process is simulated. The dimensions of the reference design are outlined in Fig. 1(b). In this reference design, two patches are strongly coupled, as illustrated by the response plotted in Fig. 2.

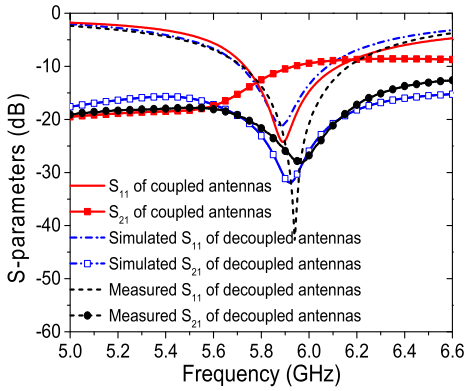

Fig. 2. Simulated and measured responses for the reference design and proposed decoupled antennas.

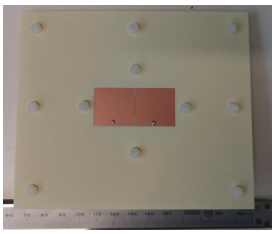

Fig. 3. Prototype of the proposed MIMO array.

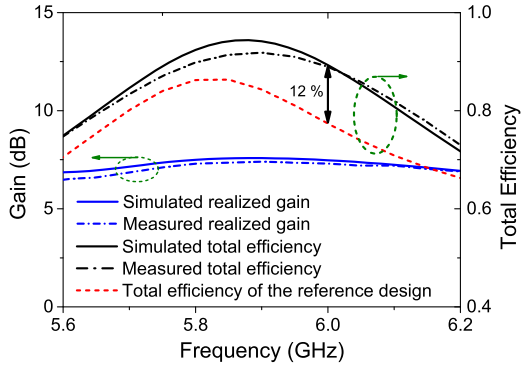

Fig. 4. Simulated and measured gain and efficiency of the antennas.

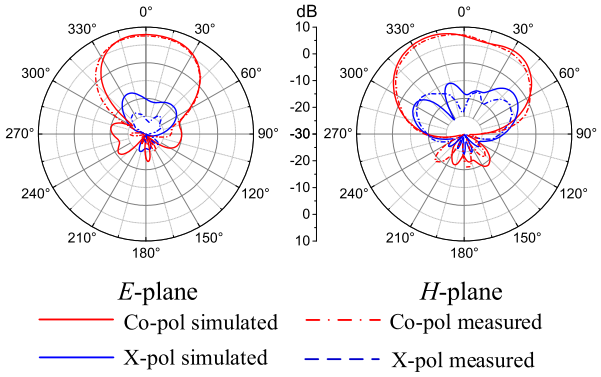

Fig. 5. Simulated and measured radiation patterns at the center frequency.

The antennas operate at a center frequency of 5.9 GHz over their fundamental TM_{10} modes. A potential application for these antennas is V2X communication (5855–5925 MHz) [30]. The total lengths of the patches in the Y-direction are approximately half-wavelength at 5.9 GHz. The edge-to-edge distance between the patches is 0.1 mm, which corresponds to $0.0018\lambda_0$ at the antenna's center frequency.

Without any modifications to the rectangular patches, the two antennas exhibit strong coupling, resulting in a low isolation of only 6.8 dB within their operating band when arranged at a distance of 0.1 mm. This strong coupling implies that a significant amount of energy will be consumed by one antenna when the other antenna is transmitting.

For the verification of the effect of the proposed novel decoupling concept, a prototype of the decoupled patch antennas is fabricated and measured with its photograph shown in Fig. 3. The ground plane size of the fabricated prototype is 110 × 130 mm. The simulated and measured S-parameters for the proposed decoupled antennas are presented in Fig. 2. The measured −10-dB bandwidth is 5.72–6.16 GHz, while the simulated bandwidth ranges from 5.71 to 6.08 GHz. The center frequency of the operating band exhibits a slight shift toward the higher frequency range due to fabrication errors.

Using the proposed decoupling technique, the measured mutual coupling between the two antennas was reduced to 18.7 dB. The only change to the proposed MIMO compared to the reference design is introducing some simple cuts at the patches' corners. With such a small change, a deep null is observed in the transmission curve of the decoupled antennas in Fig. 2, leading to a substantial improvement in isolation of up to 19.8 dB at the center frequency, compared to the coupled reference design.

Fig. 4 illustrates the simulated and measured gain and efficiency of the antennas. During the measurement process, one antenna is measured, while the other one remains terminated with a 50-Ω load. As the entire structure is symmetric, only one antenna measurement is required. The measured realized gain is 7.42 dBi, which is 7.57 dBi for the simulation. The measured total efficiency exceeds 77% within the whole operating band, with S_{11} less than −10 dB. The peak total efficiency reaches 91%. Compared to the total efficiency of the coupled antennas, a maximum improvement of 12% is observed.

Fig. 5 shows the simulated and measured radiation patterns of the proposed decoupled antennas. Due to the structural symmetry, only one antenna is measured, while the other inactive antenna is terminated with a 50-Ω wideband load. Broadside radiation is observed in both planes. The simulated and measured radiation patterns agree well. For both planes, the measured cross-polarization is lower than −16.7 and −15 dB, respectively. Because of the integrity of the ground plane, the antennas show good directional radiation for both planes with very weak backside radiation.

C. Decoupling Mechanism

To gain insight into the physical behavior of this structure, it is important to study the electric field distribution for the TM_{10} mode. Fig. 6 illustrates the electric field distribution beneath the patch for its nonradiating edges. As is known, the TM_{10} mode exhibits a half-wavelength standing wave field distribution at its two nonradiating edges. The electric field

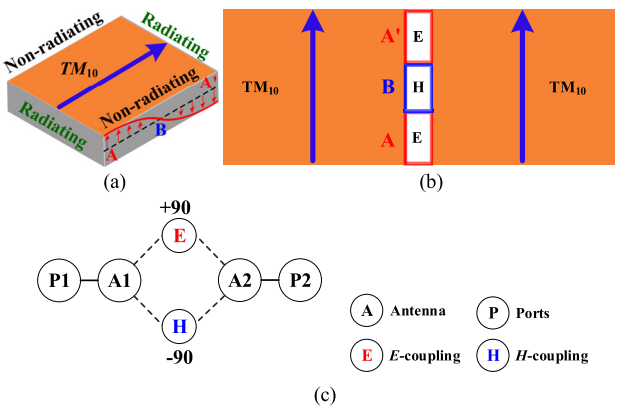

Fig. 6. (a) Electric field distribution under the patch for its fundamental TM_{10} mode. (b) Coupling behavior between two patch antennas. (c) Topology for the coupled patch antennas.

reaches its peak at the open ends of the patch (regions A and A'), while it drops to a minimum at the center (region B) [31], [32]. Conversely, a strong magnetic field distribution occurs at the virtually shorted center of the patch (region B), while it weakens at the open ends (regions A and A').

When two patches are positioned in close proximity, they will be strongly coupled through the electric (E) and magnetic (H) near fields, as depicted in Fig. 6(b). Through our study, it is found that when the separation between the patches is extremely small, the electric field dominates the mutual coupling. To mitigate the E-coupling, the four corners of the patch (regions A and A') are cut, effectively moving the electric field beneath the patches away from each other. By doing so, the E-coupling can be reduced while the weight of the H-coupling can be increased consequently. Within a certain tuning range, the E- and H-couplings become comparable in the antennas' operating band. In this specific scenario, the two coupling mechanisms cancel each other out, resulting in a low level of mutual coupling.

This EMCC behavior can be explained by the fact that electric and magnetic couplings always possess opposite signs when they coexist within the same network, as shown in Fig. 6(c) [33], [34]. This characteristic is commonly utilized in filter designs to control the positions of transmission zeros (TZs). In this work, the theory is borrowed to minimize the coupling between two patches. In filter designs, TZs are typically positioned at out-of-band frequencies to improve selectivity. However, for effective decoupling performance in antennas, the TZs must be located within the antennas' operating bands. To accomplish this, the electric and magnetic couplings should have the same magnitude. Consequently, the cuts on the patches need to be carefully designed to ensure the EMCC occurs in the frequency band of interest.

D. Parametric Study

To provide a better understanding of the design philosophy behind the proposed decoupling technique, several key parameters are investigated in this section using Ansys high-frequency structure simulator (HFSS). It is important to note that when studying one parameter, the remaining parameters are kept at the values specified in Fig. 1.

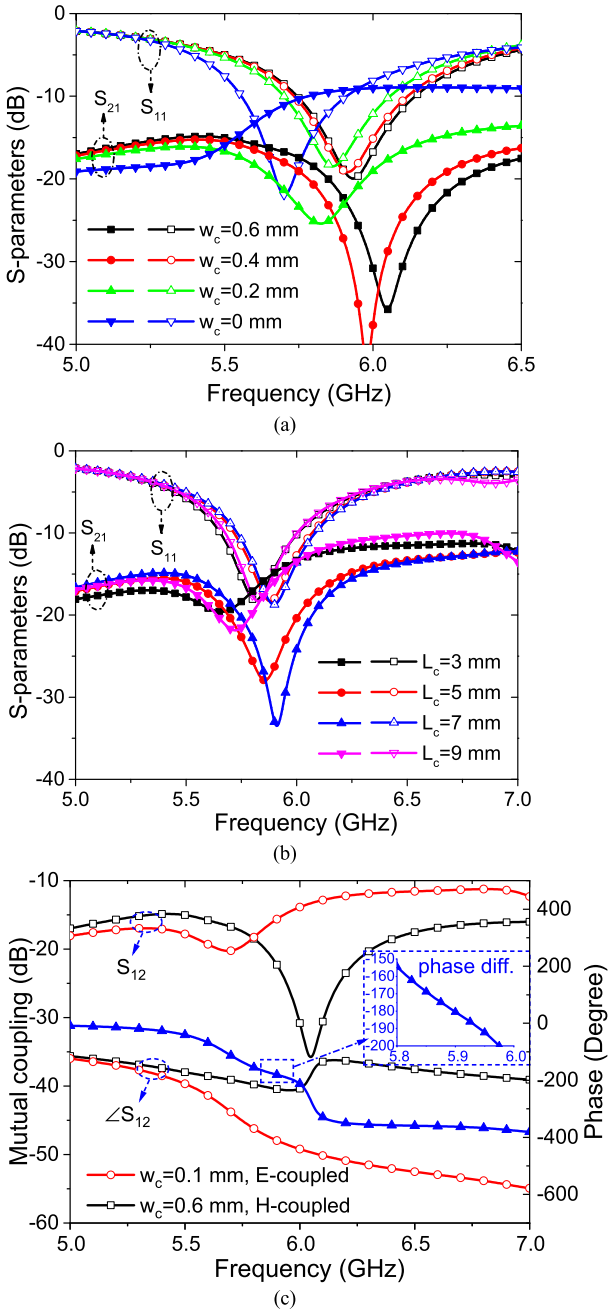

Fig. 7. Responses for the antennas with different (a) cut depths, (b) cut lengths, and (c) phase responses of the mutual couplings for E-coupled and H-coupled patches.

First, the most important parameter that affects the decoupling performance is the depth of the cut on the patch. The frequency responses for the dual-patch module with different cut depths are simulated and provided in Fig. 7(a). When there is no cut on the patch, namely, $w_c = 0$, the two patches are electrically coupled, resulting in a high transmission level between the antenna ports. According to the theory mentioned in [31], electric-coupled patches exhibit a TZ below the operating band.

As the edges of the patch are modified and the cut depth increases, the electric coupling decreases, while the magnetic coupling becomes dominant. This leads to a gradual frequency shift of the TZ to higher frequencies [31]. By carefully

designing the cut depth, the TZ can be positioned near the resonances of the antennas, resulting in a deep null in the transmission coefficient and achieving high isolation.

Another factor affecting the coupling behavior between two patches is the length of the cut on the patch (l_c). A parametric sweep is done on the cut length (l_c) with the simulated results provided in Fig. 7(b). The curves indicate that when the cut is very short ($l_c = 3$ mm), the TZ is located at a lower frequency band compared to the antenna's resonance frequency. As the cut length increases ($l_c = 5$ and 7 mm), the TZ shifts to higher frequencies. However, when the cut length exceeds an even larger value ($l_c = 9$ mm), the TZ moves back to the lower frequency band.

This phenomenon can be explained by studying the field distributions illustrated in Fig. 6. The electric field in regions A and A' is very high, so even a small variation in the cut length has a significant effect on the coupling strength related to the electric field. As the cut length increases, the electric field strength decreases, causing the TZ to shift to higher frequencies. However, when the cut reaches region B, further increasing the cut length weakens the H-coupling more than the E-coupling. Consequently, with a very long cut ($l_c = 9$ mm), the magnetic coupling may become smaller than the electric coupling again, leading to the dominance of the electric coupling mechanism. This results in the TZ moving back to the lower frequency band in terms of S-parameters. From this parametric study, an important design rule can be derived: the cut should be designed with an appropriate length. An excessively long cut can deteriorate the decoupling performance, so it is crucial to optimize the cut length to achieve the desired coupling characteristics. According to the author's experience, a cut length smaller than one-third of the patch length is recommended.

In addition to the previous studies, another important parametric study for the phase response of the mutual coupling is carried out to further reinforce the validity of the proposed decoupling concept. The results are presented in Fig. 7(c). Two cases are studied here. In the first case, where the electric coupling dominates, a shallow cut (red line with $w_c = 0.1$ mm) is implemented. Conversely, in the second case, the patches are magnetically coupled with a deeper cut (black line with $w_c = 0.6$ mm).

When the patches are electrically coupled, the TZ is at the lower frequency band. When the patches are magnetically coupled, the TZ is at the higher frequency band. The phase responses of the two cases exhibit distinct trends at the resonance frequency of the patch. Notably, the difference between the phases (*phase diff.*) is calculated and plotted in Fig. 7(c). As can be seen, the phase difference between both cases approaches approximately 180° near the resonance frequency of the patch (5.9 GHz), where the perfect EMCC occurs. This phenomenon provides strong evidence that supports the proposed decoupling concept in Section II-C.

E. Field Distributions and Design Principles

To gain a deeper understanding of the proposed decoupling concept, the field distributions at the nonradiating edges, where the coupling occurs, are investigated. Specifically, the electric

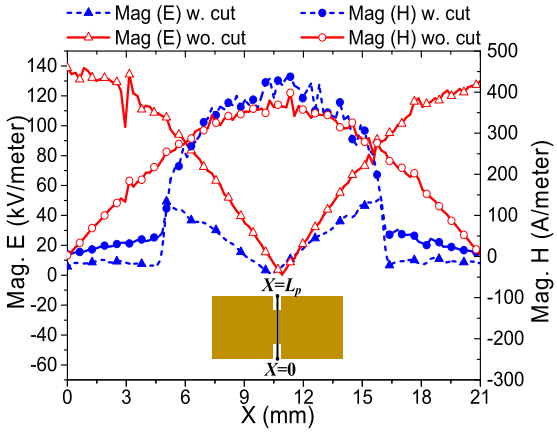

Fig. 8. Simulated E- and H-field distributions along the coupled edge.

(E, represented by red lines) and magnetic (H, represented by blue lines) field distributions are analyzed. Fig. 8 depicts the field magnitudes along a line between two patches for two different cases: one with unmodified patches (strongly coupled) and the other with decoupled patches.

In the case of strongly coupled patches without any modification, the electric and magnetic fields exhibit the behaviors described in Section II-C. Strong electric field density can be observed at the regions where $X = 0$–4.5 mm and $X = 16.5$–21 mm, which corresponds to the two open ends of the patches. When the patches' corners are cut, the field density at the open ends is significantly reduced. This reduction is more significant for the electric field because the H-field is inherently weak at the open ends. Since the fringing electric field at the nonradiating edges is weak, the magnitude of the electric field at these edges is significantly reduced when the mutual coupling is decreased, as shown in Fig. 8.

From the parametric study in Fig. 7(c), it can be seen that the mutual couplings dominated by electric and magnetic couplings are out-of-phase. As a result, when the electric and magnetic couplings are comparable, the mutual coupling between antennas can be reduced. The field distributions depicted in Fig. 8 provide insight into the underlying physical reality of the proposed decoupling process. The cuts at the ends of the nonradiating edges have a stronger effect on the electric coupling, allowing for separate control of the electric and magnetic coupling.

A basic design process can be concluded as follows. First, identify the dominating coupling mechanism of the originally coupled antennas. According to the results presented in Fig. 7(a), an H-coupled dual-patch system shows a high-band TZ, while an E-coupled one has a low-band TZ. Then, modify the edges of the patches' nonradiating edges to adjust the weights of E- and H-couplings until they are comparable. After fine-tuning, the mutual coupling level will be significantly reduced.

Current distributions on the patches are plotted in Fig. 9 with the left-hand side port excited. Strong current can be observed on both patches when they are coupled, as shown in Fig. 9(a) and (b). The current distributions indicate that the port excites both patches simultaneously because of the strong mutual coupling. After decoupling, only the

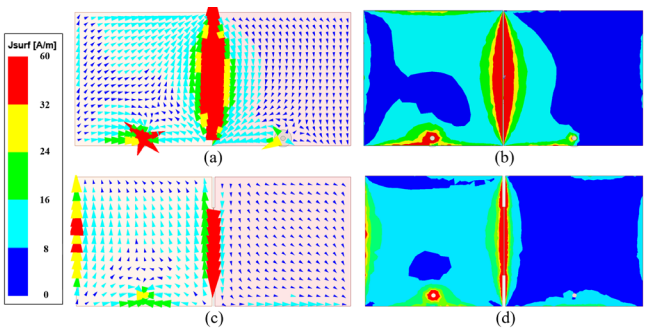

Fig. 9. Current distributions on the patches when the left-hand side patch is excited. (a) Vector plot for the coupled patches. (b) Magnitude plot for the coupled patches. (c) Vector plot for the decoupled patches. (d) Magnitude plot for the decoupled patches.

nonradiating edges of the patches, where the coupling cancellation happens, show strong current distribution. This is not strange as this method does not block the coupling between two edges. On the contrary, this phenomenon indicates that coupling cancellation happens here. Besides, the current in the other region of the coupled patch is weak, which means that the mutual coupling between the two antenna ports is small. The current distribution also indicates that only the left-hand side patch is activated when the corresponding port is excited.

F. Supplementary Case Study

To further demonstrate the effectiveness of the proposed decoupling concept, an additional case study is presented in this section. This case explores the decoupling performance of the proposed technique for two closely positioned patches utilizing only a thin dielectric substrate. A 1.5-mm Roger 4003 substrate is used here. The configuration of the decoupled antennas is illustrated in Fig. 10(a).

In this scenario, the mutual coupling between the two patches is predominantly governed by magnetic coupling. Original TZ is observed at the upper frequency range of the antennas' operating bands. Based on the theory introduced in Section II-C, the weight of electric coupling should be increased to balance the magnetic coupling. To achieve this, grooves are incorporated by cutting the central region of the nonradiating edges of the patches. This modification is particularly effective due to the presence of a strong magnetic field in this region, as highlighted in Fig. 6(b). Consequently, this alteration serves to reduce the magnetic coupling and facilitate EMCC.

The *S*-parameters of the decoupled patches are plotted in Fig. 10(b). The observed results indicate a notable enhancement in isolation between two patches, reaching 16.6 dB within the operational band, where $S_{11} < -10$ dB. In the absence of any modifications to the patches, the considerable mutual coupling diminishes the impedance matching for both antennas, as illustrated in Fig. 10(b). It is important to note that although both ports can be optimized to achieve matching, the resulting structure would operate similar to a bandpass filter with a very high mutual coupling up to −3.6 dB [35]. In this scenario, the stronger the mutual coupling, the wider the bandwidth [35]. The energy injected into one port will

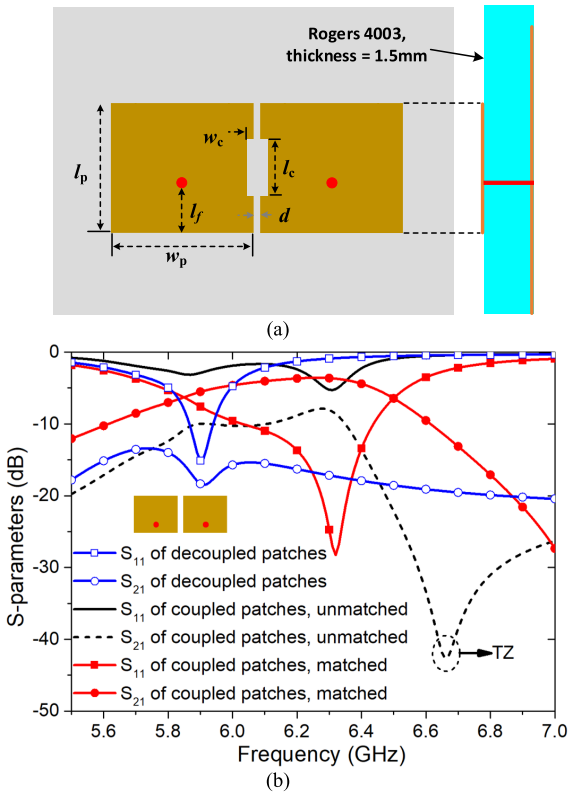

Fig. 10. Decoupled patch antennas without air substrate. (a) Structure of the decoupled patches. Dimensions in mm: $l_f = 4.75$, $l_p = 12$, $l_c = 4.5$, $w_c = 0.72$, $w_p = 13$, and $d = 0.1$. (b) Simulated responses.

mainly be transferred to another port, instead of radiating to free space. By employing the proposed technique, isolation of such two extremely strongly coupled patch antennas can be reduced with a very simple structure. Through our investigation, it is found that a bandwidth drop occurs for such a strong-coupling scenario. Consequently, this technique is not suitable for antenna systems with extremely strong mutual coupling, exceeding −3 dB, unless the designer is willing to compromise on antenna bandwidth.

III. Four-Element MIMO Array

A. Four-Element MIMO Array

The proposed EMCC decoupling concept can also be easily extended to the design of larger scale MIMO arrays. For demonstration, a four-element MIMO array is designed with the same stack-up as the previous two-element one. The structure of the four-element MIMO array is depicted in Fig. 11, where the four patches are positioned along their H-plane. Following the design concept introduced in Section II, the corners of the patches are all modified. Due to the asymmetric environment for the first antenna (ant. 1) and fourth antenna (ant. 4), these two antennas are designed with slightly different dimensions from the other two antennas at the outer sides (ant. 2 and ant. 3). The dimensions of the structure are provided in Fig. 11. The antenna is fabricated and measured. Fig. 12 presents a photograph of the fabricated antenna.

The simulated and measured *S*-parameters of the four-element MIMO array are presented in Fig. 13. The

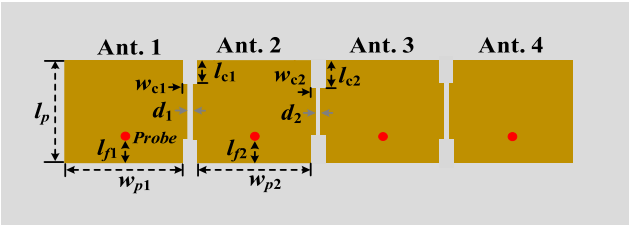

Fig. 11. Structure of the four-element MIMO array. Dimensions in mm: $lf1 = 1.05$, $lp1 = 20.4$, $lc1 = 4.65$, $lf2 = 0.6$, $lp2 = 20.4$, $lc2 = 5.65$, $wc1 = wc2 = 0.12$, $wp1 = 23.9$, $wp2 = 26.1$, $d1 = 0.85$, and $d2 = 1.45$.

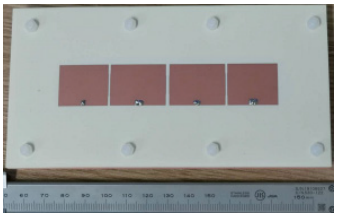

Fig. 12. Prototype of the proposed four-element MIMO array.

measured −10-dB bandwidths for ant. 1 and ant. 2 are 5.78–6.1 GHz and 5.79–6.14 GHz, respectively, while the simulated results indicate the bandwidths of 5.72–6.08 GHz and 5.74–6.09 GHz, respectively. Within their −10-dB bandwidths, the minimum isolation between these antennas is 19.3 dB. Specifically, the measured isolations between adjacent patches are 19.3 dB (S_{12}) and 20.1 dB (S_{23}), which correspond to the simulated values of 19.1 and 19.5 dB, respectively. The isolations between nonadjacent patches are 25 dB (S_{13}) and 29 dB (S_{14}), with corresponding simulated values of 26 and 32 dB, respectively. In terms of the reflection coefficients, the simulation and measurement exhibit good agreement, despite minor differences in resonance frequencies that can be attributed to fabrication errors. The isolation curves for adjacent elements agree well, while slight variations in the isolation curves for nonadjacent elements can be attributed to the sensitivity of low-magnitude transmission coefficients to the surrounding environment in the measurement.

The simulated and measured radiation patterns of the fabricated four-element MIMO are presented in Fig. 14. Two cases are measured here. Generally, broadside radiation patterns can be observed for both cases. Because no modification is introduced to the ground plane, the antennas show very low backside radiation. Besides, as only small changes are made to the geometry of the patches, good TM_{10} mode radiation is preserved for all the antennas. Thus, all these antennas show low cross-polarizations. More specifically, when ant. 1 is activated, whereas the other antennas are terminated with 50-Ω loads, the measured cross-polarization levels are 18.8 and 19 dB lower than the co-polarization for the E- and H-planes, respectively. For ant. 2, the cross-polarization levels are lower than 19.4 and 19.6 dB in the broadside direction for the E- and H-planes, respectively.

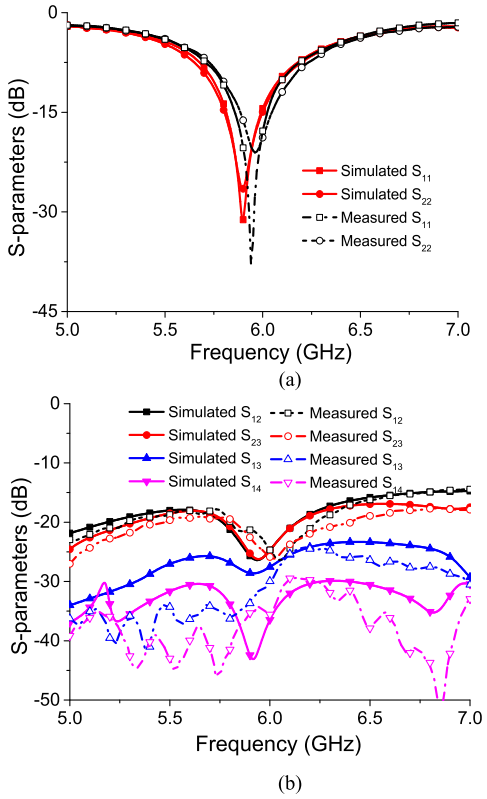

Fig. 13. Simulated and measured S-parameters for the four-element MIMO array. (a) Reflection coefficients. (b) Isolations.

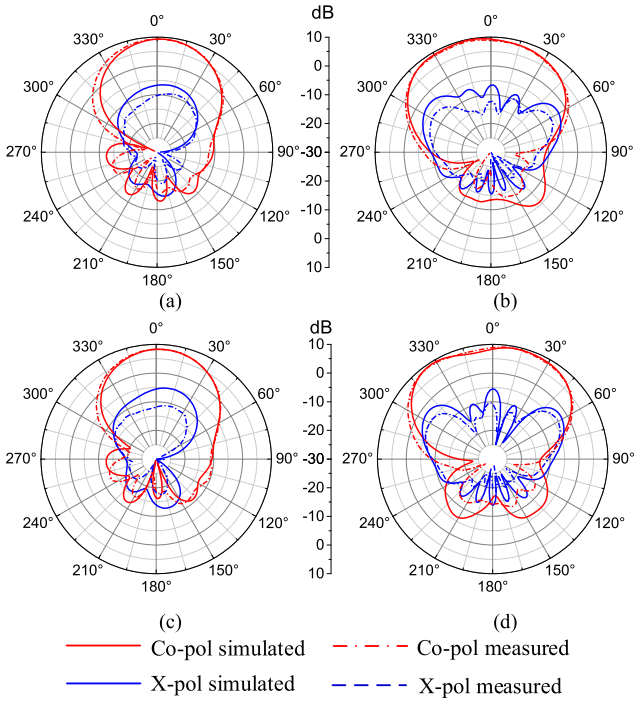

Fig. 14. Radiation patterns for the four-element MIMO array. (a) E-plane with ant. 1 excited. (b) H-plane with ant. 1 excited. (c) E-plane with ant. 2 excited. (d) H-plane with ant. 2 excited.

B. Comparison and Discussion

In Table I, the performance of the proposed EMCC decoupling method is compared to other state-of-the-art decoupling techniques. First, the proposed decoupling technique shows the simplest structure without using any additional decoupling structure [9], [10], [11], [14], additional layer [11],

TABLE I
COMPARISON OF THE PERFORMANCE BETWEEN DIFFERENT WORKS IN THE LITERATURE AND THIS WORK

Reference	Decoupling Scheme & center frequency	Complexity	Additional space for decoupling	IBD (dB)	IAD (dB)	Isolation improvement (dB)	NoE	Edge-to-edge distance (λ_0)	BW (%)	Profile (λ_0)
[9]	Resonant slot on the ground @ 5.8 GHz	Normal	Yes	N.G.	30	N.G.	2	0.031	1.7	N.G.
[10]	Slot on the ground @ 2.45 GHz	Normal	Yes	6.3	20	13.7	2	0.009	4.1	0.05
[11]	Stacked near-field resonators @ 2.45 GHz	Complex	Yes (Extra layer)	10	20/20	10	2/8	0.016/0.028	1.4/0.4	0.053
[14]	Co-planar resonator @ 3.16 GHz	Complex	Yes	7	18	11	2	0.02	1.43	0.02
[18]	Mixed modes @5.8 GHz	Normal	No	N.G.	20	N.G.	2	0.12	2.9	0.039
[19]	Weak filed @3.5 GHz	Normal	No	24	30	6	2	0.18	N.G.	0.037
[20]	Higher-order mode operation @ 5.25 GHz	Normal	Yes	8.2	20.2/21.5	12	2 / 4	0.007 / 0.02	4/3.6	0.063
[21]	Structural parameter @ 5 GHz	Normal	No	17	24.6	7.4	2	0.033	6.6	0.054
[24]	Inductors @ 2.45 GHz	Multiple steps	Yes (Dummy patches)	5	15.4/12.2	10.4/7.2	2/4	0.016	5.5/3.5	0.049
This work	Modified patches @ 5.9 GHz	Simple	NO	6.8	18.7	11.9	2	0.0018	7.4	0.065
					19.3	12.5	4	0.026	6	

N.G.: not given; IBD: Isolation before decoupling; IAD: Isolation after decoupling; NoE: Number of Elements; BW: Bandwidth

or increased antenna area [20]. Some of these presented designs also suffer from the time-consuming design process. In contrast, our proposed EMCC method has an extremely simple design flow. From the parametric studies carried out in Section II-D, designers only need to pay attention to two key parameters during the decoupling process.

Second, the proposed two-element MIMO design achieves the smallest antenna separation, which is only 0.002 free-space wavelength. For the isolation level, the proposed technique ensures a general mutual coupling of up to 18.7 dB within the band of interest, with a minimum isolation improvement of 11.9 dB. Although the isolation performance in [9] is higher than this value, the decoupling method in [9] requires a long slot on the ground plane. Besides, the decoupling ability of this resonating slot is very sensitive to the ground size. These limitations make it not suitable for applications, where system ground plane integrity is important.

It is also worth mentioning that the proposed technique is different from the common and differential modes cancellation (CDMC) technique reported in [23] and [24]. In the CDMC process, the common and differential modes of the dual-antenna system must be tuned to have similar status regarding their impedance characteristics and resonance frequencies. To achieve this, extra design processes are needed. For example, in [23], the ground size, antenna height, and antenna width must be carefully designed to match the impedance characteristics of both common and differential modes. In [24], additional dummy antenna elements are needed to balance the loading effects of every patch antenna. In contrast, the EMCC method in our work is more flexible and simpler in design, more compact, and more cost-efficient.

Furthermore, when compared to other self-decoupled patch antennas presented in previous works [18], [19], [20], [21], the proposed technique exhibits the smallest edge-to-edge distance along with enhanced design flexibility. In contrast, the methods outlined in [18], [19], and [20] need specific patch-to-patch distances and predetermined structures. Similarly, the approach presented in [21] is constrained by limitations associated with the dielectric constant of the substrates and the inherent isolation levels.

The proposed EMCC concept is also verified as effective for both two-element and four-element MIMO arrays. Regarding the specific design examples presented in this article, the proposed method shows the widest decoupling bandwidth compared to other presented works. Some decoupling techniques require resonating structure to accomplish reduced mutual coupling in the band of interest. Nevertheless, a resonant structure always shows frequency-relevant impedance characteristics, which means that these decoupling structures may only work well in a limited frequency range. This explains why some decoupled antennas show very narrow impedance bandwidths [9], [11], [14].

In summary, considering the size, fabrication complexity, decoupling ability, and antenna separation, the proposed technique provides a very attractive decoupling solution for small-separation multiantenna systems.

IV. Conclusion

This article presents a novel decoupling solution for patch antennas positioned in extremely close proximity along their H-planes. The proposed EMCC technique eliminates the need for additional decoupling structures or layers by introducing very simple modifications to the patch structure itself. The effectiveness of the concept is demonstrated through the design and analysis of both two-element and four-element MIMO arrays. Comparative evaluations against the existing state-of-the-art decoupling techniques highlight several advantages of the proposed method, including its simplicity in structure, cost-effectiveness, and suitability for applications requiring minimal antenna separation. In summary, the proposed decoupling solution offers a promising approach to address the mutual coupling challenges in closely placed patch antennas, showing promising application prospects in various wireless communication systems for enhanced performance and improved system integration.

References

[1] E. Rajo-Iglesias et al., "Mutual coupling reduction in patch antenna arrays by using a planar EBG structure and a multilayer dielectric substrate," *IEEE Trans. Antennas Propag.*, vol. 56, no. 6, pp. 1648–1655, Jun. 2008.

[2] F. Yang and Y. Rahmat-Samii, "Microstrip antennas integrated with electromagnetic band-gap (EBG) structures: A low mutual coupling design for array applications," *IEEE Trans. Antennas Propag.*, vol. 51, no. 10, pp. 2936–2946, Oct. 2003.

[3] S. Ghosal, A. De, R. M. Shubair, and A. Chakrabarty, "Analysis and reduction of mutual coupling in a microstrip array with a magneto-electric structure," *IEEE Trans. Electromagn. Compat.*, vol. 63, no. 5, pp. 1376–1383, Oct. 2021.

[4] A. Askarian, J. Yao, Z. Lu, and K. Wu, "Surface-wave control technique for mutual coupling mitigation in array antenna," *IEEE Microw. Wireless Compon. Lett.*, vol. 32, no. 6, pp. 623–626, Jun. 2022.

[5] J.-G. Yook and L. P. B. Katehi, "Micromachined microstrip patch antenna with controlled mutual coupling and surface waves," *IEEE Trans. Antennas Propag.*, vol. 49, no. 9, pp. 1282–1289, Sep. 2001.

[6] K. S. Vishvaksenan, K. Mithra, R. Kalaiarasan, and K. S. Raj, "Mutual coupling reduction in microstrip patch antenna arrays using parallel coupled-line resonators," *IEEE Antennas Wireless Propag. Lett.*, vol. 16, pp. 2146–2149, 2017.

[7] A. Habashi, J. Nourinia, and C. Ghobadi, "Mutual coupling reduction between very closely spaced patch antennas using low-profile folded split-ring resonators (FSRRs)," *IEEE Antennas Wireless Propag. Lett.*, vol. 10, pp. 862–865, 2011.

[8] C.-Y. Chiu, C.-H. Cheng, R. D. Murch, and C. R. Rowell, "Reduction of mutual coupling between closely-packed antenna elements," *IEEE Trans. Antennas Propag.*, vol. 55, no. 6, pp. 1732–1738, Jun. 2007.

[9] J. OuYang, F. Yang, and Z. M. Wang, "Reducing mutual coupling of closely spaced microstrip MIMO antennas for WLAN application," *IEEE Antennas Wireless Propag. Lett.*, vol. 10, pp. 310–313, 2011.

[10] S. Zhang, B. K. Lau, Y. Tan, Z. Ying, and S. He, "Mutual coupling reduction of two PIFAs with a T-shape slot impedance transformer for MIMO mobile terminals," *IEEE Trans. Antennas Propag.*, vol. 60, no. 3, pp. 1521–1531, Mar. 2012.

[11] M. Li, B. G. Zhong, and S. W. Cheung, "Isolation enhancement for MIMO patch antennas using near-field resonators as coupling-mode transducers," *IEEE Trans. Antennas Propag.*, vol. 67, no. 2, pp. 755–764, Feb. 2019.

[12] Y. Cheng, X. Ding, W. Shao, and B. Wang, "Reduction of mutual coupling between patch antennas using a polarization-conversion isolator," *IEEE Antennas Wireless Propag. Lett.*, vol. 16, pp. 1257–1260, 2017.

[13] J. Andersen and H. Rasmussen, "Decoupling and descattering networks for antennas," *IEEE Trans. Antennas Propag.*, vol. AP-24, no. 6, pp. 841–846, Nov. 1976.

[14] T. Pei, L. Zhu, J. Wang, and W. Wu, "A low-profile decoupling structure for mutual coupling suppression in MIMO patch antenna," *IEEE Trans. Antennas Propag.*, vol. 69, no. 10, pp. 6145–6153, Oct. 2021.

[15] Y.-M. Zhang, S. Zhang, J.-L. Li, and G. F. Pedersen, "A wavetrap-based decoupling technique for 45° polarized MIMO antenna arrays," *IEEE Trans. Antennas Propag.*, vol. 68, no. 3, pp. 2148–2157, Mar. 2020.

[16] Y.-M. Zhang et al., "A simple decoupling network with filtering response for patch antenna arrays," *IEEE Trans. Antennas Propag.*, vol. 69, no. 11, pp. 7427–7439, Nov. 2021.

[17] L. Zhao, L. K. Yeung, and K.-L. Wu, "A novel second-order decoupling network for two-element compact antenna arrays," in *Proc. Asia Pacific Microw. Conf.*, Dec. 2012, pp. 1172–1174.

[18] Q. X. Lai, Y. M. Pan, S. Y. Zheng, and W. J. Yang, "Mutual coupling reduction in MIMO microstrip patch array using TM_{10} and TM_{02} modes," *IEEE Trans. Antennas Propag.*, vol. 69, no. 11, pp. 7562–7571, Nov. 2021.

[19] H. Lin, Q. Chen, Y. Ji, X. Yang, J. Wang, and L. Ge, "Weak-field-based self-decoupling patch antennas," *IEEE Trans. Antennas Propag.*, vol. 68, no. 6, pp. 4208–4217, Jun. 2020.

[20] J.-F. Qian, S. Gao, B. S. Izquierdo, H. Wang, H. Zhou, and H. Xu, "Mutual coupling suppression between two closely placed patch antennas using higher order modes," *IEEE Trans. Antennas Propag.*, vol. 17, no. 6, pp. 4686–4694, Jun. 2023.

[21] L.-L. Yang, X.-F. Wang, Y.-H. Ke, W.-W. Yang, and J.-X. Chen, "Dielectric patch antenna self-decoupling by proper structural parameters," *IEEE Antennas Wireless Propag. Lett.*, vol. 21, pp. 1447–1451, 2022.

[22] M. Li, S. Tian, M.-C. Tang, and L. Zhu, "A compact low-profile hybrid-mode patch antenna with intrinsically combined self-decoupling and filtering properties," *IEEE Trans. Antennas Propag.*, vol. 70, no. 2, pp. 1511–1516, Feb. 2022.

[23] L. Sun, Y. Li, Z. Zhang, and H. Wang, "Antenna decoupling by common and differential modes cancellation," *IEEE Trans. Antennas Propag.*, vol. 69, no. 2, pp. 672–682, Feb. 2021.

[24] L. Sun, Y. Li, and Z. Zhang, "Decoupling between extremely closely spaced patch antennas by mode cancellation method," *IEEE Trans. Antennas Propag.*, vol. 69, no. 6, pp. 3074–3083, Jun. 2021.

[25] X. M. Yang, X. G. Liu, X. Y. Zhou, and T. J. Cui, "Reduction of mutual coupling between closely packed patch antennas using waveguided metamaterials," *IEEE Antennas Wireless Propag. Lett.*, vol. 11, pp. 389–391, 2012.

[26] H. King, "Mutual impedance of unequal length antennas in echelon," *IRE Trans. Antennas Propag.*, vol. 5, no. 3, pp. 306–313, Jul. 1957.

[27] N. Alexopoulos and I. Rana, "Mutual impedance computation between printed dipoles," *IEEE Trans. Antennas Propag.*, vol. AP-29, no. 1, pp. 106–111, Jan. 1981.

[28] A. Derneryd, "A theoretical investigation of the rectangular microstrip antenna element," *IEEE Trans. Antennas Propag.*, vol. AP-26, no. 4, pp. 532–535, Jul. 1978.

[29] D. Pozar, "Input impedance and mutual coupling of rectangular microstrip antennas," *IEEE Trans. Antennas Propag.*, vol. AP-30, no. 6, pp. 1191–1196, Nov. 1982.

[30] H. Ullah, N. G. Nair, A. Moore, C. Nugent, P. Muschamp, and M. Cuevas, "5G communication: An overview of vehicle-to-everything, drones, and healthcare use-cases," *IEEE Access*, vol. 7, pp. 37251–37268, 2019.

[31] J.-F. Qian, F.-C. Chen, Q.-X. Chu, Q. Xue, and M. J. Lancaster, "A novel electric and magnetic gap-coupled broadband patch antenna with improved selectivity and its application in MIMO system," *IEEE Trans. Antennas Propag.*, vol. 66, no. 10, pp. 5625–5629, Oct. 2018.

[32] X. Chen, J. Wang, and L. Chang, "Extremely low-profile dual-band microstrip patch antenna using electric coupling for 5G mobile terminal applications," *IEEE Trans. Antennas Propag.*, vol. 71, no. 2, pp. 1895–1900, Feb. 2023.

[33] J.-S. Hong and M. J. Lancaster, "Couplings of microstrip square open-loop resonators for cross-coupled planar microwave filters," *IEEE Trans. Microw. Theory Techn.*, vol. 44, no. 11, pp. 2099–2109, Nov. 1996.

[34] J. B. Thomas, "Cross-coupling in coaxial cavity filters—A tutorial overview," *IEEE Trans. Microw. Theory Techn.*, vol. 51, no. 4, pp. 1368–1376, Apr. 2003.

[35] J.-S. Hong and S. Li, "Theory and experiment of dual-mode microstrip triangular patch resonators and filters," *IEEE Trans. Microw. Theory Techn.*, vol. 52, no. 4, pp. 1237–1243, Apr. 2004.

Jianfeng Qian (Graduate Student Member, IEEE) received the B.S. degree from Hefei University of Technology, Hefei, China, in 2016, and the M.E. degree from the South China University of Technology, Guangzhou, China, in 2019. He is currently pursuing the Ph.D. degree with the University of Kent, Canterbury, U.K.

His research interests include microwave antennas, filters, filtering antennas, and associated RF circuits for microwave and millimeter-wave applications.

Mr. Qian was a recipient of the Outstanding Master's Thesis Award from the Chinese Institute of Electronics in 2019 and the Best Student Paper Award from the 17th International Workshop on Antenna Technology (iWAT 2022), Dublin.

Benito Sanz Izquierdo (Member, IEEE) received the B.Sc. degree from ULPGC, Las Palmas, Spain, and the M.Sc. and Ph.D. degrees from the University of Kent, Canterbury, U.K.

In 2012, he worked at Harada Industries Ltd., Birmingham, U.K., where he developed novel antennas for the automotive industry. He was a Research Associate with the School of Engineering, University of Kent, where he became a Lecturer in electronic systems in 2013 and a Senior Lecturer in 2018. His research interests include multiband antennas, wearable electronics, additive manufacturing (3-D printing), substrate integrated waveguides components, metamaterials, sensors, electromagnetic bandgap structures, frequency-selective surfaces, and reconfigurable devices.

Steven Gao (Fellow, IEEE) received the Ph.D. degree from Shanghai University, Shanghai, China, in 1999.

He was a Post-Doctoral Research Fellow with the National University of Singapore, Singapore, a Research Fellow with Birmingham University, Birmingham, U.K., a Visiting Research Scientist at the Swiss Federal Institute of Technology, Zürich, Switzerland, a Visiting Fellow at Chiba University, Chiba, Japan, a Visiting Scientist at the University of California, Santa Barbara, CA, USA, a Senior Lecturer, a Reader, and the Head of the Antenna and Microwave Group, Northumbria University, Newcastle upon Tyne, U.K., and the Head of the Satellite Antennas and RF System Group, Surrey Space Centre, University of Surrey, Surrey, U.K. He is currently a Professor and the Chair of RF and Microwave Engineering with the University of Kent, Canterbury, U.K. Since 1994, he has been with China Research Institute of Radiowave Propagation, Xinjiang, China. He has been a Professor with the University of Kent, since 2013. He has coauthored *Circularly Polarized Antennas* (IEEE-Wiley, 2014), over 250 papers and several patents. His current research interests include smart antennas, phased arrays, MIMO, satellite antennas, microwave/mm-wave/THz circuits, satellite and mobile communications, and radar (UWB radar and synthetic-aperture radar) and wireless power transfer.

Dr. Gao is a Fellow of IET, U.K. He was a Coeditor of the *Space Antenna Handbook* (Wiley, 2012). He was a General Chair of LAPC 2013 and an Invited or Keynote Speaker of some international conferences, such as the AES'2014, the IWAT'2014, the SOMIRES'2013, and the APCAP'2014. He is an IEEE AP-S Distinguished Lecturer, an Associate Editor of the IEEE TRANSACTIONS ON ANTENNAS AND PROPAGATION, an Associate Editor of *Radio Science*, and an Editor in-Chief of the Wiley Book Series on *Microwave and Wireless Technologies*.

Hanyang Wang (Fellow, IEEE) received the Ph.D. degree from Heriot-Watt University, Edinburgh, U.K., in 1995.

From 1986 to 1991, he was a Lecturer and an Associate Professor with Shandong University, Jinan, China. From 1995 to 1999, he was a Post-Doctoral Research Fellow with the University of Birmingham, Birmingham, U.K., and the University of Essex, Colchester, U.K. From 1999 to 2000, he was with Vector Fields Ltd., Oxford, U.K., as a Software Development and Microwave and Antenna Engineering Consultant Engineer. He joined Nokia U.K. Ltd., Farnborough, U.K. in 2001, where he was a Mobile Antenna Specialist for 11 years. He was an Adjunct Professor at Nanjing University, Nanjing, China, from 2019 to 2022. He joined Huawei, Shenzhen, China, after leaving Nokia U.K. Ltd., where he is currently the Chief Scientist of mobile terminal antennas. He leads a large group of antenna experts and engineers and takes the full leadership and responsibility in the research and development of antenna technologies to guarantee the market success of all Huawei's mobile terminal products ranging from smartphones, laptops, tablets, MiFi, data cards, smart watches, BT headsets, routers, the Internet of Things, smart screens, CPE, VR, and automobiles. He has been an Adjunct Professor at Sichuan University, Chengdu, China, since 2011. He has authored over referred 130 papers on these topics. He holds more than 50 granted US/EU/JP/CN patents, including 32 US patents, and has more than 80 patent applications in pending. His current research interests include small, wideband, multiband antennas and MIMO antennas for mobile terminals and antenna arrays for 5G sub-6 GHz and 5G millimeter-wave mobile communications.

Dr. Wang is a Huawei Fellow and an IET Fellow. He was a recipient of the Title of Nokia Inventor of the Year in 2005, the Nokia Excellence Award in 2011, the Huawei Individual Gold Medal Award in 2012, and the Huawei Team Gold Medal Award in 2013 and 2014, respectively. His patent was ranked number one among 2015 Huawei top ten patent awards. He was an Associate Editor of IEEE ANTENNAS AND WIRELESS PROPAGATION LETTERS from 2015 to 2021.

Hai Zhou received the Ph.D. degree in reflector antenna synthesis from the University of London, London, U.K., in 1987.

He carried out his Post-Doctoral work with the University of London, until 1992. He served as a Senior Lecturer with London South Bank University, London, working on GSM, UMTS, and LTE in system engineering. He joined Lucent Technologies, Wiltshire, U.K., in 1996. He joined Huawei Technologies, Reading, U.K., in 2015. He worked on various topics from shaped reflector antenna synthesis, FDTD during his academic years to radio resource management and adaptive antennas in industry. He has authored or coauthored 14 journal articles and 34 conference articles. He holds 18 patents.

Dr. Zhou was a recipient of the Best Paper Award from the 19th European Microwave Conference in 1989 and received the Oliver Lodge Premium from IEE as the Best Paper of the Year on Antennas and Propagation in 1991.

Huiliang Xu was born in Leshan, Sichuan, China. He received the B.S. degree in applied geophysics from China University of Mining and Technology, Xuzhou, Jiangsu, China, in 1998, the M.S. degree in optics from South China Normal University, Guangzhou, China, in 2005, and the Ph.D. degree in optical engineering from the Institute of Optics and Electronics, Chinese Academy of Sciences, Chengdu, Sichuan, in 2008.

From 1998 to 2002, he was a Petroleum Logging Engineer with China Petroleum Logging Company Ltd., Xi'an, China. In October 2008, he joined Huawei Technologies Company Ltd., Shenzhen, China, where he is the Wireless Terminal Antenna Expert. His current research interests include metal reconfigurable antenna, wearable antennas, vehicle-mounted antenna, metamaterial antenna, and antenna system simulation.